Available online at www.sciencedirect.com

SciVerse ScienceDirect

Journal of the European Ceramic Society 32 (2012) 1605–1611

www.elsevier.com/locate/jeurceramsoc

Chemical oxidation of residual carbon from $ZnAl_2O_4$ powders prepared by combustion synthesis

Robert Ianoş *, Radu Lazău, Ioan Lazău, Cornelia Păcurariu

"Politehnica" University of Timişoara, Faculty of Industrial Chemistry and Environmental Engineering, P-ţa Victoriei No. 2, Timişoara 300006, Romania

Received 23 November 2011; accepted 13 December 2011
Available online 24 January 2012

Abstract

The removal of carbon residue from $ZnAl_2O_4$ nanopowders by annealing at 500–800 °C leads to a decrease of specific surface area from 228.1 m^2/g to 47.6 m^2/g. At the same time, the average crystallite size increased from 5.1 nm to 14.9 nm. In order to overcome these drawbacks, a new solution for removing the carbon residue has been suggested: chemical oxidation using hydrogen peroxide. In terms of carbon removal, a H_2O_2 treatment for 8 h at 107 °C proved to be equivalent to a heat treatment of 1 h at 600 °C. The benefits of chemical oxidation over thermal oxidation were obvious. The specific surface area was much larger (188.1 m^2/g) in the case of the powder treated with H_2O_2. The average crystallite size (5.8 nm) of $ZnAl_2O_4$ powder treated with H_2O_2 was smaller than the crystallite size (8.2 nm) of the $ZnAl_2O_4$ powder annealed at 600 °C.

Keywords: Powders-chemical preparation; Spinels; Sensors; Grain size; Carbon oxidation

1. Introduction

The removal of carbon residue from ceramic powders prepared by "soft chemical routes" has always been a delicate issue. Usually, the complete removal of carbon by annealing under air atmosphere requires not only a sufficiently high temperature (usually above 700 °C) but also a significant period of time (several hours).

On the other hand, there are many literature reports describing various "soft chemical routes" of preparing high reactivity ceramic nanopowders: citrate,[1–3] combustion synthesis,[4,5] Pechini,[6,7] sol–gel,[8–11] organic precursors,[12] etc. The efficiency of these methods can be assessed in terms of lower annealing temperature, shorter soaking time and superior characteristics of the resulting product (nanocrystalline character, large specific surface area, small grain size, lower agglomeration degree).

For instance, it is reported that $ZnAl_2O_4$, frequently used in organic syntheses for its catalytic activity, may be obtained at 500–600 °C by using the citrate method.[3] However, the as-prepared powders cannot be pressed and then sintered due to the presence of large amount of residual carbon originating from the incomplete oxidation of the organic material. Although the formation of the $ZnAl_2O_4$ takes place at ≈550 °C, the complete removal of the residual carbon requires a heat treatment of 2 h at 800 °C.[3]

The preparation of α-Al_2O_3, corundum, powder by thermal decomposition of complex combination derived from sucrose and aluminum nitrate is another eloquent example. According to the results reported by Das et al.,[13] after annealing the sucrose–aluminum nitrate precursor at 600 °C for 4 h a gray powder of α-Al_2O_3 is obtained. In this case, the complete removal of carbon material can be achieved only after a heat treatment of 12 h at 600 °C.[13]

Powder annealing at temperatures 200 °C higher than the minimum temperature where the designed crystalline phase is formed leads to the decrease of specific surface area and amplifies grain growth and agglomeration phenomena.

In this context, the present paper suggests an innovative and rational solution, which reduces the temperature and duration of heat treatment required for the removal of residual carbon. Basically, the solution reported hereby relies on treating the ceramic powder which contains residual carbon with a concentrated solution of hydrogen peroxide, followed by drying.

* Corresponding author. Fax: +40 403060.
E-mail address: robert_ianos@yahoo.com (R. Ianoş).

0955-2219/$ – see front matter © 2011 Elsevier Ltd. All rights reserved.
doi:10.1016/j.jeurceramsoc.2011.12.028

Table 1
Raw materials used in the present experiments.

Sample	$Zn(NO_3)_2{\cdot}4H_2O$	$Al(NO_3)_3{\cdot}9H_2O$	$C_6H_{18}N_4$	H_2O_2
Manufacturer	Merck	Merck	Riedel-de Haën	Silal trading
Purity	Pro analysi	Pro analysi	Pro analysi	Pro analysi
M (g/mol)	261.44	375.13	146.24	34.01
c (%)	≥98.5	≥98.5	–	30
ρ (g/cm^3)	–	–	0.98	–

2. Experimental procedure

2.1. Combustion synthesis of $ZnAl_2O_4$ powder

Table 1 shows the starting raw materials, which were used for solution combustion synthesis of $ZnAl_2O_4$ powder. The $Zn(NO_3)_2$:$Al(NO_3)_3$:$C_6H_{18}N_4$ molar ratio of 7:14:20 corresponds to a $C_6H_{18}N_4$ (triethylenetetramine) excess of 300%.

The recipe was designed in order to obtain 70.0 g of $ZnAl_2O_4$. After dosing and mixing the starting materials (Fig. 1) in distilled water, a clear solution was obtained. In the next step, the porcelain dish containing the precursor solution has been placed in a heating mantle, preheated at 400 °C. As the temperature of the precursor solution increases, most of the water evaporates and an exothermic combustion reaction occurs. During this process, which takes for about five minutes, the raw material mixture reaches a dark red incandescence and large amounts of gases evolve, typical for smoldering combustion. The fluffy material which resulted after the combustion process ended was hand-crushed with a pestle, resulting in a black powder (denoted as sample A). Small portions of sample A were annealed for 1 h at temperatures ranging from 500 °C to 800 °C.

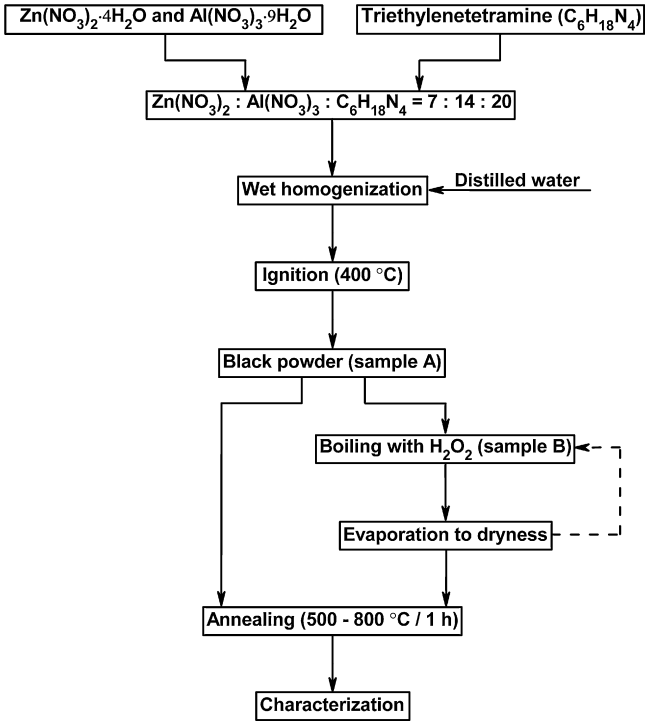

Fig. 1. The general preparation scheme of $ZnAl_2O_4$ powders.

Another portion of the black powder resulted from the combustion reaction (sample A), was treated with a concentrated solution of hydrogen peroxide, H_2O_2, followed by heating at 107 °C under continuous magnetic stirring at 500 rpm. For every gram of powder, 20.0 mL of H_2O_2 were used. After 8 h, the color of the powder treated with H_2O_2 (denoted as sample B) turned from black to light gray and the sample was evaporated to dryness. Subsequently, small portions of powder B were annealed in the same conditions as sample A (Fig. 1).

2.2. Characterization techniques

The heating behavior of samples A and B was monitored by thermal analysis, using a Netzsch 449 C instrument equipped with Pt crucibles. The TG–DTA curves were recorded under an artificial air flow of 20 mL/min, at a heating rate of 10 °C/min.

The carbon, nitrogen and hydrogen content of the powders (CNH elemental analysis) was determined by "Dynamic Flash Combustion" using an Elemental Analyzer EA 1108 according to ASTM D 5373-08 standard test procedures.

The phase composition of the powders was determined by X-ray diffraction, using a Panalytical XPERT-PRO diffractometer operating at 45 kV and 30 mA. The X-ray diffraction patterns were recorded using the Ni filtered $Cu_{K\alpha}$ radiation. The crystallite size was calculated based on the Scherrer's equation (1), using the fallowing h k l peaks: 3 1 1, 2 2 0 and 4 4 0.

$$D_{XRD} = \frac{0.9 \cdot \lambda}{\beta \cdot \cos\ \theta} \quad (1)$$

where: D_{XRD} is the crystallite size (nm), λ stands for the radiation wavelength (0.15406 nm), β is the full width at half of the peak (radians), θ is the Bragg angle (degrees).

The lattice parameter of cubic $ZnAl_2O_4$ was calculated based on the X-ray diffraction patterns, using Eq. (2):

$$a = d_{hkl}(h^2 + k^2 + l^2) \quad (2)$$

where: a is the lattice parameter (Å), d is the interplanar distance (Å) and hkl are the Miller indices of the peaks (3 1 1, 2 2 0 and 4 4 0).

BET (Brunauer–Emmet–Teller) specific surface area of the powders was measured by N_2(g) adsorption technique using a Micromeritics ASAP 2020 instrument. The equivalent grain diameter was calculated based on the BET specific surface area (3):

$$D_{BET} = \frac{6000}{\rho \cdot S} \quad (3)$$

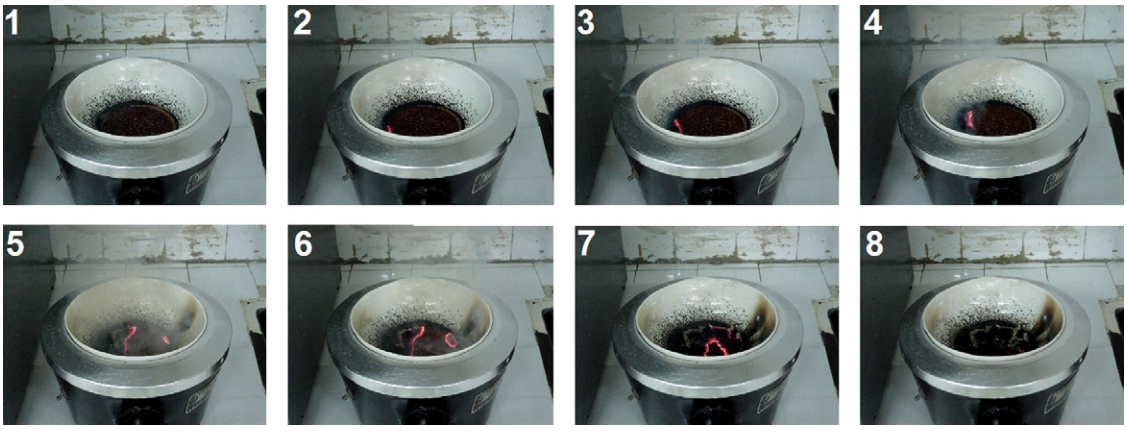

Fig. 2. Digital images recorded during the preparation of $ZnAl_2O_4$ powder by combustion synthesis.

where: D_{BET} is the equivalent grain diameter (nm), ρ is the theoretical density of $ZnAl_2O_4$ (4.62 g/cm^3) and S stands for the BET specific surface area (m^2/g).

The two series of powders were also characterized by Fourier-transform infrared spectroscopy, using a Shimadzu PRESTIGE-21 FT–IR spectrometer in the range of 400–4000 cm^{-1} with KBr pellets.

The color of the samples was investigated by diffuse reflectance spectrophotometry. CIEL*a*b* parameters were measured using a Varian Cary 300 Bio UV-VIS spectrophotometer (illuminant – D_{65}, observer angle – 10°). L* is a measure of brightness: L* = 100 corresponds to the total reflection of radiation from the VIS range (white), whilst L* = 0 corresponds to the complete absorption of radiation from the VIS range (black). Negative values of a* indicates the proportion of green. Positive values of a* indicates the proportion of red. Negative values of b* indicates the proportion of blue. Positive values of b* indicates the proportion of yellow.

3. Results and discussion

The combustion reaction evolved as a typical smoldering process (Fig. 2), meaning that the reaction front propagated very slowly. The combustion temperature was not very high, as the sample hardly reached incandescence. The powder obtained at the end of the combustion process had a black color, which indicates the presence of residual carbon (Table 2), derived from partial oxidation of triethylenetetramine. The CNH elemental analysis of the sample resulted from the combustion process (Table 2) confirmed that the powder contains 6.1% carbon as well as small amounts of nitrogen (2.8%) and hydrogen (1.0%).

3.1. Thermal analysis investigations

Thermal analysis of the precursor solution containing $Zn(NO_3)_2$, $Al(NO_3)_3$ and $C_6H_{18}N_4$ (Fig. 3) reveals that up to 100 °C, the sample undergoes an endothermic process (82 °C), which is accompanied by a mass loss of about 18%. Most probably, the phenomenon occurring in this case is the elimination of water from the aqueous solution.

As the temperature increases, the ignition of the combustion reaction occurs. This process is characterized by a steep and significant mass loss on the TG curve (Fig. 3) which is accompanied by a sharp exothermic effect on the DTA curve (294 °C). Since the black powder resulting from the combustion has a carbon content of 6.1% (Table 2), one can assume that the second exothermic effect (471 °C) – which is also accompanied by a mass loss – may be assigned to burning out the residual carbon (thermal oxidation). The shape of TG and DTA curves suggests that above 500 °C sample undergoes no further transformations.

Thermal analysis of the black powder prepared by combustion synthesis (sample A) indicates that during heating 3 major processes occur (Fig. 4). The DTA curve of sample A shows an endothermic effect at 125 °C, which is accompanied by a mass loss on the TG curve, corresponding to the removal of the adsorbed moisture. Another process occurs at 227 °C and it is characterized by a slight mass loss on the TG curve, which may be related to a small exothermic reaction between traces of amorphous metal nitrates and triethylenetetramine.

The presence of traces of amorphous metal nitrates and triethylenetetramine in the powder resulted from the combustion reaction is supported by the CNH elemental analysis (Table 2),

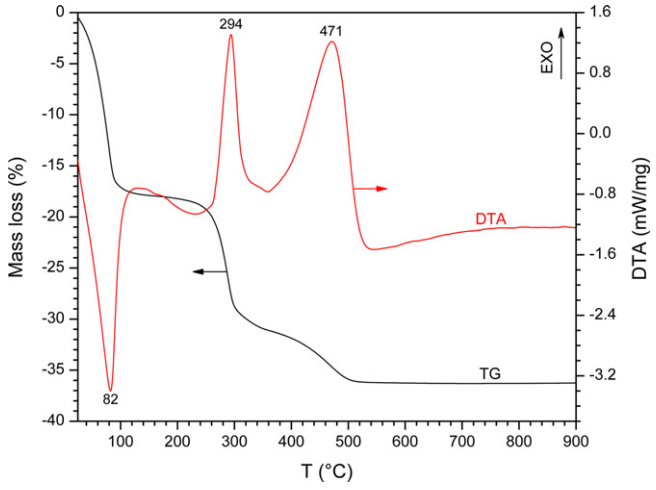

Fig. 3. TG–DTA curves of the precursor solution consisting of $Zn(NO_3)_2$, $Al(NO_3)_3$ and $C_6H_{18}N_4$.

Table 2
CNH elemental analysis, lattice parameter, crystallite size, specific surface area and the equivalent grain size of the samples.

Sample	CNH elemental analysis [wt.%]			a[a] [Å]	D_{XRD}[b] [nm]	S[c] [m^2/g]	D_{BET}[d] [nm]	D_{BET}/D_{XRD}
	C	N	H					
A	6.1	2.8	1.0	8.089	5.1	228.1	5.7	1.14
A_{500}	0.5	0.1	0.7	–	–	160.3	8.1	–
A_{600}	0.4	0.1	0.4	8.087	8.2	113.0	11.5	1.40
A_{800}	–	–	–	8.084	14.9	47.6	27.3	1.83
B	0.4	0.8	1.3	8.087	5.8	188.1	6.9	1.19
B_{500}	0.3	0.1	0.7	–	–	164.1	7.9	–
B_{600}	0.2	0.1	0.6	8.085	7.4	133.7	9.7	1.31
B_{800}	–	–	–	8.083	13.2	67.5	19.2	1.45

[a] Lattice parameter.
[b] Crystallite size.
[c] Specific surface area.
[d] Equivalent grain diameter.

which indicated that sample A contained 6.1% carbon as well as small amounts of nitrogen (2.8%) and hydrogen (1.0%). As the temperature increases, the DTA curve exhibits a broad exothermic effect in the temperature range of 300–600 °C (with a maximum at 484 °C), which is assigned to burning out the residual carbon (thermal oxidation). The removal of residual carbon is marked on the TG curve as a significant mass loss (Fig. 4).

After 8 h of mixing and heating at 107 °C, the color of the powder treated with H_2O_2 (sample B) turned from black to light gray (Fig. 5). Considering that pure $ZnAl_2O_4$ is white, this color change suggests that the sample treated with hydrogen peroxide (sample B) contains less carbon residue than the mother sample A.

The CNH elemental analysis confirms these results (Table 2): the mother sample A has a carbon content of 6.1% whilst the sample treated with H_2O_2 (sample B) has a carbon content of only 0.4%. Obviously, the carbon content decreased radically, which indicates that hydrogen peroxide, H_2O_2, was able to chemically oxidize the residual carbon. As a matter of fact in the field of soil analysis hydrogen peroxide is often used as a pretreatment reagent for organic matter removal.[14,15] However, this would be for the first time when hydrogen peroxide is used for the removal of carbon residue from ceramic nanopowders, as there are no such reports in the literature.

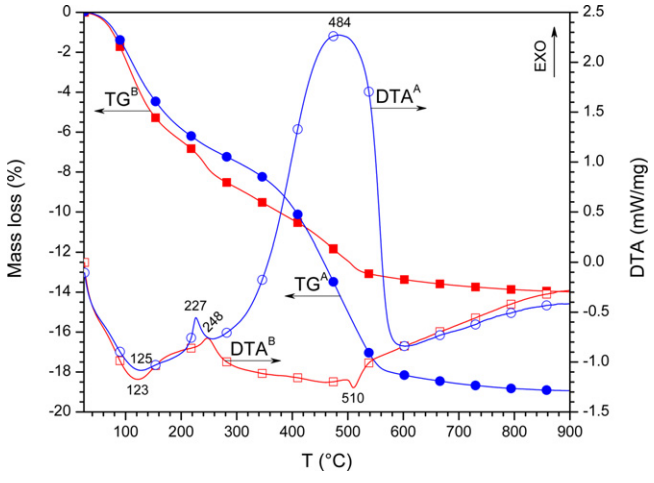

Fig. 4. TG–DTA curves of powders A and B.

Thermal analysis of the sample treated with H_2O_2 (sample B) revealed that over the temperature range of 25–300 °C, the TG–DTA curves of sample B (Fig. 4) resemble quite well the TG–DTA curves of sample A. However, instead of a broad exothermic effect, which appears on the DTA curve at 484 °C (denoting the residual carbon burnout), the DTA curve shows only a small endothermic effect at 510 °C, indicating a possible decomposition process.

Besides the visible color change of the powder treated with H_2O_2 (Fig. 5), the TG curves of samples A and B revealed an important difference between the total mass loss of the two samples. From this point of view, one may notice that the total mass loss of sample B (13.9%) is significantly smaller than the total mass loss of sample A (18.9%), which confirms once more the carbon removal during the hydrogen peroxide treatment (Fig. 4).

3.2. XRD characterization

X-ray diffraction analysis revealed that the only crystalline phase present in the powder resulting from the combustion reaction (sample A) is the spinel-structured $ZnAl_2O_4$, known as gahnite (Fig. 6). The average crystallite size of $ZnAl_2O_4$ is 5.1 nm. Based on the results obtained by X-ray diffraction and the CNH analysis of sample A, one can assume that the combustion synthesized powder is a mixture of $ZnAl_2O_4$ and amorphous carbon. After annealing the A powder at 600 °C and 800 °C for 1 h, a slight increase of the crystallite size could be observed, to 8.2 nm and 14.9 nm (Table 2).

The XRD pattern of sample B is very similar to the one of sample A (Fig. 6), indicating that $ZnAl_2O_4$ is the only crystalline phase. The average crystallite size of $ZnAl_2O_4$ is 5.8 nm. Therefore, in terms of phase composition, there is virtually no difference between powder A and powder B, treated with H_2O_2. After annealing powder B at 600 °C and 800 °C for 1 h, a slight increase of the crystallite size could be observed, to 7.4 nm and 13.2 nm respectively (Table 2).

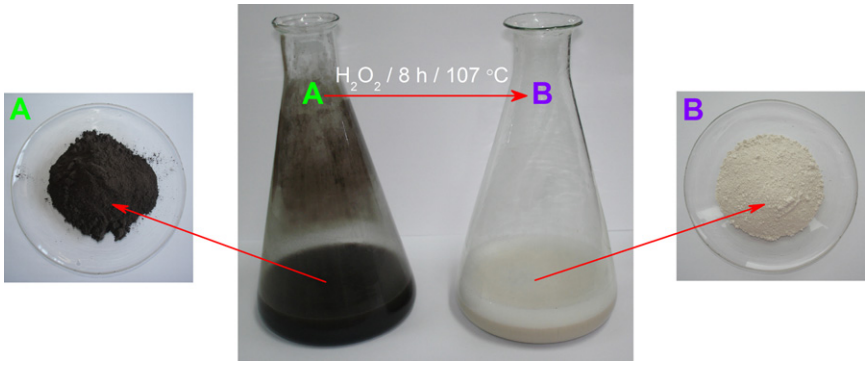

Fig. 5. Digital images of powders A and B.

3.3. Specific surface area measurements

After performing the sample degassing operation at 400 °C, the specific surface area of sample A (228.1 m^2/g) proved to be larger than the specific surface area of sample B (188.1 m^2/g) (Table 2). Taking into account the CNH elemental analysis (Table 2), this decrease of the specific surface area may be explained by the removal of fine carbon fraction as a result of H_2O_2 treatment. The removal of small carbon grains by H_2O_2 oxidation is also supported by the evolution of cumulative pore volume, which decreases from 0.33 cm^3/g (sample A) to 0.28 cm^3/g (sample B).

Fig. 7 shows the evolution of specific surface area and equivalent grain diameter of samples A and B as a function of the annealing temperature. As the annealing temperature increases, the carbon content of the samples decreases, but so does the specific surface area (Table 2). In this case, the traditional carbon removal by annealing (thermal oxidation) has major side effects on the other powder properties, such as specific surface area and grain size. In order to reach the same carbon content as the sample treated with H_2O_2 (sample B), mother sample requires annealing at 600 °C for 1 h (sample A_{600}) (Table 2).

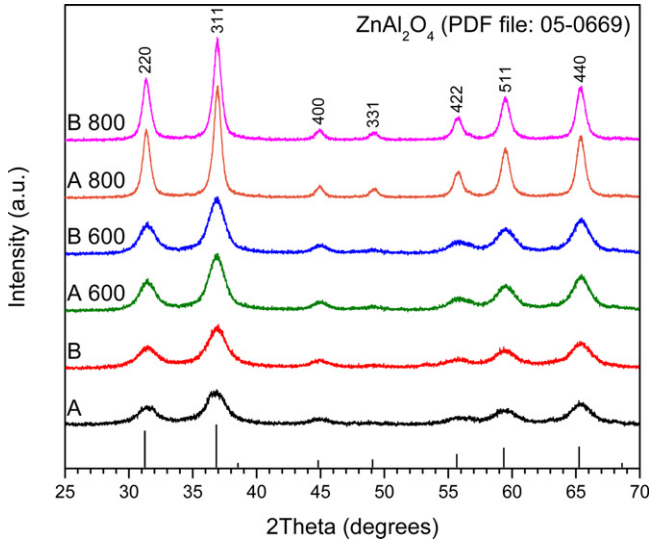

Fig. 6. XRD patterns of samples A and B before and after annealing 1 h at 600 °C and 800 °C.

However, the specific surface area of sample B is 188.1 m^2/g, whilst the specific surface area of sample A_{600} decreased by almost 40%, to 113.0 m^2/g. Therefore, the solution we report hereby allows the elimination of carbon residue by H_2O_2 chemical oxidation, without altering the other powder properties.

On the other hand, the specific surface area of both samples (A and B) decreases as the annealing temperature increases (Fig. 7). Yet, the specific surface area decreases to a higher extent in the case of sample A. Moreover, it is quite obvious that above 500 °C, the specific surface of sample B is larger than the one of sample A. Even at 800 °C, powder B has a specific surface of 67.5 m^2/g, which is ≈42% higher than the specific surface area of sample A, 47.6 m^2/g (Table 2).

In the case of both sample series (A and B), the equivalent grain diameter increases with increasing the annealing temperature. The evolution of equivalent grain diameter as a function of temperature suggests that A grains are growing much faster than B grains. At 800 °C the A grains (27.3 nm) are ≈42% larger than the B grains (19.2 nm).

3.4. FT-IR investigations

FT-IR spectra of samples A and B, before and after annealing for 1 h at 600 °C and 800 °C are shown in Fig. 8. The large

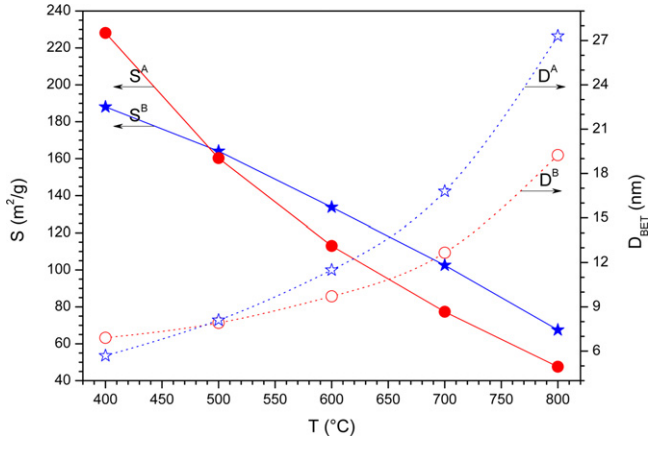

Fig. 7. The evolution of specific surface area and equivalent grain diameter of samples A and B as a function of the annealing temperature.

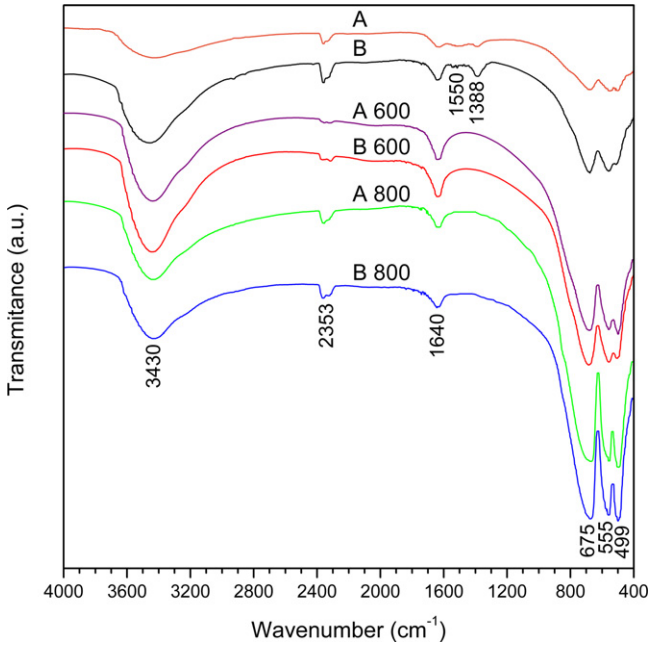

Fig. 8. FT-IR spectra of samples A and B, before and after annealing 1 h at 600 °C and 800 °C.

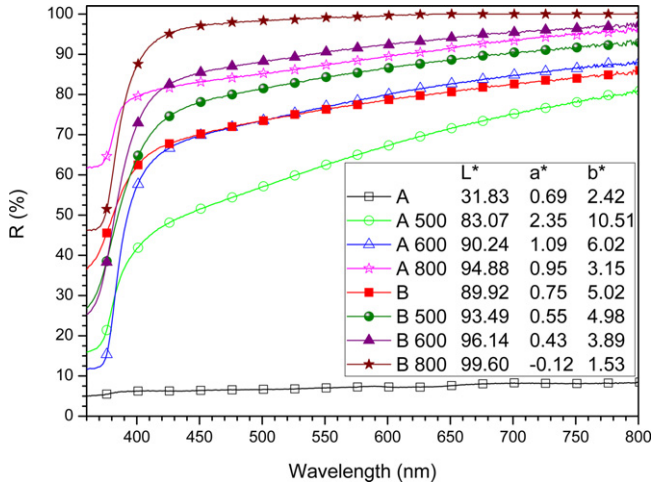

Fig. 9. DRS spectra and CIEL*a*b* parameters of samples A and B before and after annealing at various temperatures.

specific surface area of the powders enables the rapid adsorption of H_2O and CO_2 from the atmosphere, as evidenced by the FT-IR spectra of the samples (Fig. 8). The broad band at 3430 cm^{-1} may be assigned to the stretching vibration of H_2O molecules, whilst the band from 1640 cm^{-1} is attributed to H_2O bending.

The absorption band at 2353 cm^{-1} is due to the stretching vibration of CO_2. The bands at 675, 555 and 499 cm^{-1} confirm the formation of normal spinel structure, $ZnAl_2O_4$, as evidenced by the XRD analysis (Fig. 6). The band at 1388 cm^{-1} may be assigned to nitrate anion, which suggests that combustion reaction did not reach completion.

Considering that an excess of triethylenetetramine has been used, it is likely that small amounts of triethylenetetramine may also exist within powders A and B, which agrees with the CNH elemental analysis (Table 2).

Whilst the presence of $-NH_2$ stretch band (around 3400 cm^{-1}) cannot be clearly identified on the FT-IR spectra of samples A and B because of its overlapping with the H_2O stretch band, one may observe the bending vibration of $-NH_2$ group at 1550 cm^{-1}. Furthermore, as shown by the TG–DTA analysis of samples A and B (Fig. 4), the combustion reaction between traces of metal nitrates and triethylenetetramine is responsible for the small exothermic effect, which occurs at 227–248 °C.

From this point of view, there is an excellent correlation of the TG–DTA results (Fig. 4) and the disappearance of nitrate and $-NH_2$ bands (1388 cm^{-1} and 1550 cm^{-1} respectively) after annealing at 600 °C. On the other hand, as the annealing temperature increases the typical bands of $ZnAl_2O_4$ (675, 555 and 499 cm^{-1}) increase in intensity, which indicates a more advanced crystallinity degree of $ZnAl_2O_4$, in agreement with the XRD analysis (Fig. 6).

3.5. CIEL*a*b* measurements

The influence of the H_2O_2 treatment and the annealing temperature on the color of samples A and B has been studied by means of diffuse reflectance spectroscopy and CIEL*a*b* parameters (Fig. 9). The black color of sample A, which contains 6.1% carbon, is illustrated by the intense unselective absorption of the VIS radiation (Fig. 9) and the low value of the brightness parameter, $L^* = 31.83$. On the other hand, after the H_2O_2 treatment, sample B, which contains 0.4% carbon, shows much higher value of the brightness parameter, $L^* = 89.92$ (Fig. 9), which is in agreement with the light gray color of the powder (Fig. 5).

After analyzing the CIEL*a*b* parameters shown in Fig. 9, one may notice that the brightness, L^*, increases as the annealing temperature increases, due to the removal of carbon residue. The samples treated with H_2O_2 show higher brightness and higher reflectance than the samples A annealed at the same temperature. Actually, in terms of brightness there are only minor differences between sample B and sample A_{600} annealed at 600 °C for 1 h.

In terms of color and carbon content (Table 2), a hydrogen peroxide treatment of 8 h at 107 °C (sample B) is virtually equivalent to a heat treatment applied to sample A_{600} of 1 h at 600 °C. In terms of other measurable properties of the powder, such as specific surface area or equivalent grain size diameter, the balance tilts in favor of sample B, which allows obtaining powders with smaller grain size and higher specific surface are (Table 2). In addition, the D_{BET}/D_{XRD} ratio suggests that the agglomeration degree of A crystallites is higher than the agglomeration degree of B crystallites, which means that the number of crystallites in A grains is higher than the number of crystallites in B grains.

4. Conclusions

Carbon impurified $ZnAl_2O_4$ resulted from the combustion reaction of zinc nitrate, aluminum nitrate and triethylenetetramine. The removal of carbon residue by annealing at

temperatures of 500–800 °C promoted a substantial decrease of specific surface area from 228.1 m^2/g to 47.6 m^2/g. At the same time, an increase of the average crystallite size was noticed, from 5.1 nm to 14.9 nm.

In order to overcome these drawbacks a new solution to remove the carbon residue from $ZnAl_2O_4$ powders has been suggested. This alternative relies on the chemical oxidation of carbon residue by hydrogen peroxide rather than thermal oxidation (annealing).

In terms of color, the CIEL*a*b* measurements indicated that an H_2O_2 treatment for 8 h at 107 °C is equivalent to a heat treatment of 1 h at 600 °C. The benefits of chemical oxidation instead of thermal oxidation of residual carbon were obvious.

The specific surface area of the powder treated with H_2O_2 was much larger (188.1 m^2/g) than the specific surface area of the powder annealed at 600 °C (113.0 m^2/g). At the same time, the crystallite size (5.8 nm) and the equivalent grain size diameter (6.9 nm) of the powder treated with H_2O_2 were smaller when compared to the crystallite size (8.2 nm) and the equivalent grain size diameter (11.5 nm) of the powder annealed at 600 °C.

Acknowledgement

This work was supported by a grant of the Romanian National Authority for Scientific Research, CNCS–UEFISCDI, project number PN-II-RU-TE-2011-3-0024 (18/05.10.2011).

References

1. Chen L, Sun X, Liu Y, Zhou K, Li Y. Porous $ZnAl_2O_4$ synthesized by a modified citrate technique. *J Alloy Compd* 2004;**376**:257–61.
2. Li X, Zhua Z, Zhaoa Q, Wang L. Photocatalytic degradation of gaseous toluene over $ZnAl_2O_4$ prepared by different methods: a comparative study. *J Hazard Mater* 2011;**186**:2089–96.
3. Duan X, Yuan D, Sun Z, Luan C, Pan D, Xu D, et al. Preparation of Co^{2+}-doped $ZnAl_2O_4$ nanoparticles by citrate sol–gel method. *J Alloy Compd* 2005;**386**:311–4.
4. Visinescu D, Jurca B, Ianculescu A, Carp O. Starch – a suitable fuel in new low-temperature combustion-based synthesis of zinc aluminate oxides. *Polyhedron* 2011;**30**:2824–31.
5. Viana KMS, Dantas BB, Nogueira NAS, Carp JM, Freitas NL, Kiminami RHGA, et al. Influence of fuel in the synthesis of $ZnAl_2O_4$ catalytic supports by combustion reaction. *Mater Sci Forum* 2010;**660–661**:52–7.
6. Wu Y, Wang X. Preparation and characterization of single-phase α-Fe_2O_3 nano-powders by Pechini sol–gel method. *Mater Lett* 2011;**65**:2062–5.
7. Silva D, Abreu A, Davolos MR, Rosaly M. Determination of the local site occupancy of Eu^{3+} ions in $ZnAl_2O_4$ nanocrystalline powders. *Opt Mater* 2011;**33**:1226–33.
8. Davar F, Salavati-Niasari M. Synthesis and characterization of spinel-type zinc aluminate nanoparticles by a modified sol–gel method using new precursor. *J Alloy Compd* 2011;**509**:2487–92.
9. Kurajica S, Tkalcec E, Sipusic J, Matijasic G, Brnardic I, Simcic I. Synthesis and characterization of nanocrystalline zinc aluminate spinel by sol–gel technique using modified alkoxide precursor. *J Sol-Gel Sci Technol* 2008;**46**:152–60.
10. Da Silva AA, de Souza Gonçalves A, Davolos MR. Characterization of nanosized $ZnAl_2O_4$ spinel synthesized by the sol–gel method. *J Sol-Gel Sci Technol* 2009;**49**:101–5.
11. Xiuhua W, Donghua C. Synthesis and characterization of nanosized zinc aluminate spinel by sol–gel technique. *Mater Lett* 2006;**60**:823–7.
12. Nikumbh AK, Adhyapak PV. Synthesis, properties and optimization of the rheological behaviors on alumina and zinc aluminate powders obtained from dicarboxylate precursors. *Powder Technol* 2010;**202**:14–23.
13. Das RN, Bandyopadhyay A, Bose S. Nanocrystalline α-Al_2O_3 using sucrose. *J Am Ceram Soc* 2001;**84**:2421–3.
14. Mikutta R, Kleber M, Kaiser K, Jahn R. Organic matter removal from soils using hydrogen peroxide, sodium hypochlorite, and disodium peroxodisulfate. *Soil Sci Soc Am J* 2005;**69**:120–35.
15. Bissey LL, Smith JL, Watts RJ. Soil organic matter–hydrogen peroxide dynamics in the treatment of contaminated soils and groundwater using catalyzed H_2O_2 propagations (modified Fenton's reagent). *Water Res* 2006;**40**:2477–84.